Available online at www.sciencedirect.com
ScienceDirect
International Journal of Heat and Mass Transfer 50 (2007) 4311–4322
International Journal of HEAT and MASS TRANSFER
www.elsevier.com/locate/ijhmt

Optimal control of flow in solar collectors for maximum exergy extraction

Viorel Badescu *

Candida Oancea Institute, Faculty of Mechanical Engineering, Polytechnic University of Bucharest, Spl. Independentei 313, Bucharest 79590, Romania

Received 7 March 2006; received in revised form 12 December 2006
Available online 9 May 2007

Abstract

The best operation strategies for open loop flat-plate solar collector systems are considered. A direct optimal control method (the TOMP algorithm) is implemented. A detailed collector model and realistic meteorological data from both cold and warm seasons are used in applications. The maximum exergetic efficiency is low (usually less than 3%), in good agreement with experimental measurements reported in literature. The optimum mass-flow rate increases near sunrise and sunset and by increasing the fluid inlet temperature. The optimum mass-flow rate is well correlated with global solar irradiance during the warm season. Also, operation at a properly defined constant mass-flow rate may be close to the optimal operation.

Keywords: Flow rate optimization; Exergy; Flat-plate solar collector; Optimal control

1. Introduction

Solar radiation is an important source of exergy. Fully concentrated direct solar radiation is very rich in exergy (more than 90%) [1,2]. The exergy content of fully concentrated diffuse solar radiation is smaller but still high, ranging from 72.6% for single scattering to 9.6% in case of four scatterings [3]. Therefore, solar energy collection systems may be used for power generation. Part of the incident exergy flux is of course lost inside the solar energy conversion equipment due to various irreversible processes (for a recent study see [4]). Maximizing the exergy gain finally means minimizing the effects of these irreversible processes. It is known that thermal energy storage is associated to exergy destruction [5–8]. Therefore, the energy storage should normally be avoided in solar thermal systems designed for power generation. Open loop should be preferred to closed loop configurations in this case. Note that storage units are usually included in solar energy conversion systems designed for direct thermal energy utilization.

Solar energy conversion strategies are different from the point of view of their costs and feasibility. Optimization of these conversion processes can yield a variety of answers, depending not only on the objective of the optimization but also on the constraints that define the problem. More specifically, the optimal paths are different when maximization of exergy gain rather than energy gain is of interest. Early approaches on energy gain maximization through mass-flow rate control are reported by Kovarik and Lesse [9], Horel and De Winter [10] and Bejan and Schultz [11]. More recently, Hollands and Brunger [12] dealt with the water flow rate optimization for a closed loop system. Additional comments may be found in De Winter [13]. Different objective functions (all of them related to the energy gain) were considered by these authors. For instance, the minimum cost per unit of energy transferred was considered in [10] while in [12] the amount of collected energy was maximized. Different optimal strategies were found when the exergy gain was analyzed (see [14]).

This paper refers to optimal operation strategies for exergy gain maximization by using open loop flat-plate solar collector systems. The water mass-flow rate in the collectors is the control parameter. Three are the novelties of

* Fax: +40 21 410 4251.
E-mail address: badescu@theta.termo.pub.ro

0017-9310/$ - see front matter © 2007 Elsevier Ltd. All rights reserved.
doi:10.1016/j.ijheatmasstransfer.2007.01.061

Nomenclature

A_c	solar energy collection surface area [m^2]
A'_t	heat transfer surface area per unit collection area
c_m	specific heat of plate material [J kg^{-1} K^{-1}]
c_p	fluid specific heat [J kg^{-1} K^{-1}]
E_x	exergy [J]
$\widetilde{E}$	dimensionless exergy defined by Eq. (10)
$\dot{E}_x$	exergy flux [W]
G	solar global irradiance [W m^{-2}]
g	dimensionless solar global irradiance defined by Eq. (8b)
h_f	convection heat transfer coefficient between pipes and fluid [W m^{-2} K^{-1}]
$\tilde{h}$	dimensionless convection heat transfer coefficient defined by Eq. (9c)
M'	collector plate surface mass density [kg m^{-2}]
$\dot{m}$	mass-flow rate [kg s^{-1}]
$\dot{m}'$	mass-flow rate per unit collection surface area [kg m^{-2} s^{-1}]
T	temperature, spatially averaged collector plate temperature [K]
T_{amb}	ambient temperature [K]
t	time [s]
$\widetilde{U}$	dimensionless overall heat loss coefficient defined by Eq. (9b)
U_L	collector's overall heat loss coefficient [W m^{-2} K^{-1}]
w_{wind}	wind speed [m s^{-1}]

Greek symbols

η	efficiency
$\bar{\eta}$	time averaged efficiency
μ	dimensionless flow rate factor defined by Eq. (9d)
θ	dimensionless temperature, dimensionless plate temperature defined by Eq. (8c)
τ	dimensionless time defined by Eq. (8a)
$(\tau\alpha)$	effective transmittance–absorptance product
$(\widetilde{\tau\alpha})$	normalized effective transmittance–absorptance product defined by Eq. (9a)

Subscripts

1,2	related to integration times
en	energy
ex	exergy
f	fluid
i	inlet
m	mean
opt	optimum
out	outlet
ref	reference
x	exergy

our approach. First, a realistic solar collector model is used. This should be compared to the very simple collector models used previously in [9,11,14]. Additional simplifying assumptions were adopted in the quoted papers to make the problem mathematically tractable by using rather simple time-dependent optimization procedures. The hypothesis of constant-(in-time) coefficients (i.e. collector's effective transmittance–absorptance product and overall heat loss coefficient) was such a simplification. Numerical optimization techniques are used here. They allowed developing a more realistic mathematical model with time-dependent coefficients. This is our second improvement. Third, the model was implemented by using a large meteorological database. This makes the results more credible than the results of previous approaches where implementations were performed without using measured series of meteorological parameters.

Flow rate control is an important factor to increase the performance of solar thermal systems. In general, the controller must be able to vary the manipulated variable (i.e. the flow rate) in accordance with two types of fluctuations in the controlled variable (which is a temperature usually). One type of fluctuation is attributed to disturbances while another is caused by occurrences of overshoots and undershoots in the manipulated variables that are caused by a lack of knowledge of future events [15]. Controllers for objective functions others than the solar energy gain were less studied in literature. A few aspects concerning controller design in case the objective function is the exergy gain will be presented here.

2. Meteorological and actinometric data

Meteorological data measured in Bucharest (latitude 45.5° N, longitude 26.2° E, altitude 131 m above sea level) by the Romanian Meteorological and Hydrological Institute are used in this work [16]. The climate of Bucharest is temperate – continental with a climatic index of continentality (Ivanov) of 131.9%. The METEORAR database consists of values measured at 1.00, 7.00, 13.00 and 19.00 local standard time (LST) for ambient temperature, air relative humidity and point cloudiness. Also, the database contains daily average values for the atmospheric pressure.

The following computation procedure is adopted here to evaluate meteorological and actinometric data for a given moment during the day. The temperature is interpolated linearly between neighboring measured data from the METEORAR database. The global solar irradiance is next

evaluated on a horizontal surface by using the model we proposed in [17]. The entries for this model are the point cloudiness, the ambient temperature, the atmospheric pressure and the air relative humidity. A simple isotropic model is subsequently used to evaluate the direct, diffuse and ground-reflected solar irradiance on a tilted surface by using as input the fluxes of solar energy incident on a horizontal surface (see, e.g. [18]). The ground albedo is always assumed to be 0.2 [19].

The typical meteorological year assumption is adopted (see e.g. [20]). This allows meteorological data from a single year (i.e. 1961) to be used in computations [7]. The seasonally averaged wind speed is as follows: $w_{\text{wind}} = 1.8\ \text{m s}^{-1}$ (warm season, i.e. April–October in the Northern hemisphere) and $w_{\text{wind}} = 2.48\ \text{m s}^{-1}$ (cold season, i.e. November–March).

3. Transient solar energy collection model

A registry-type flat-plate solar collector is considered in this study. The effective transmittance–absorptance product and the overall heat loss coefficient are denoted $(\tau\alpha)$ and U_{L}, respectively. Both quantities may depend on temperature or on the time-dependent working conditions. The material of the collector plate has a surface mass density M' and specific heat c_{m}. The surface collection area is denoted A_{c}. The specific heat and mass-flow rate of the working fluid is c_p and $\dot{m}$, respectively. The fluid enters and leaves the collection area at temperature $T_{\text{f,i}}$ and $T_{\text{f,out}}$, respectively. The incident solar irradiance and the ambient temperature are denoted G and T_{amb}, respectively.

The temperature of the collector plate depends on space and time. The present model uses an absorber plate temperature (denoted T) averaged at the level of the whole surface area. All (space averaged) collector properties are evaluated as a function of this space averaged temperature (see [21,22] for details). Table 1 gives the values adopted for various parameters describing the flat-plate solar collector treated in this paper.

The energy balance at the level of the absorber plate yields:

$$M' A_{\text{c}} c_{\text{m}} \frac{\text{d}T}{\text{d}t} = (\tau\alpha) G A_{\text{c}} - U_{\text{L}} A_{\text{c}} (T - T_{\text{amb}}) - \dot{m}' A_{\text{c}} c_p (T_{\text{f,out}} - T_{\text{f,i}}) \quad (1)$$

Here $\dot{m}' (\equiv \dot{m}/A_{\text{c}})$ is the mass-flow rate per unit collection surface area. One denotes by h_{f} and A'_{t} the convection heat transfer coefficient between collector pipes and fluid and the heat transfer surface area per unit collection area, respectively. The next assumption is that the (space averaged) pipe wall temperature equals the plate temperature T. Then, the following steady-state energy balance equation applies:

$$h_{\text{f}} A'_{\text{t}} A_{\text{c}} (T - T_{\text{f,m}}) = \dot{m}' A_{\text{c}} c_p (T_{\text{f,out}} - T_{\text{f,i}}) \quad (2)$$

Table 1
Values adopted for the flat-plate solar collector treated in this paper

Quantity	Value
Transparent cover	
Number of transparent layers	1
Thickness of one transparent layer	0.004 m
Relative refraction index	1.526
Absorption coefficient (water white glass)	$4\ \text{m}^{-1}$
Emittance	0.88
Absorber plate (aluminium)	
Thickness	0.0015 m
Absorptance	0.9
Emittance	0.1
Thermal conductivity	$211\ \text{W m}^{-1}\ \text{K}^{-1}$
Mass density	$2700\ \text{kg m}^{-3}$
Specific heat	$896\ \text{J kg}^{-1}\ \text{K}^{-1}$
Distance between tubes	0.1 m
Tube external diameter	0.013 m
Tube internal diameter	0.01 m
Bond conductance	$0.03\ \text{m K W}^{-1}$
Bottom thermal insulation (polyurethane)	
Thickness	0.05 m
Thermal conductivity	$0.034\ \text{W m}^{-1}\ \text{K}^{-1}$
Working fluid (water)	
Specific heat	$4185\ \text{J kg}^{-1}\ \text{K}^{-1}$
Mass density	$1000\ \text{kg m}^{-3}$

In Eq. (2), $T_{\text{f,m}}$ is a (space averaged) fluid temperature defined in first approximation by

$$T_{\text{f,m}} \equiv \frac{T_{\text{f,i}} + T_{\text{f,out}}}{2} \quad (3)$$

Fig. 1 (associated to Fig. 5) shows as an example the time dependence of various collector parameters during July. The effective transmittance–absorptance product $(\tau\alpha)$ is rather constant during the day, with some decrease near sunrise and sunset (Fig. 1e). The overall heat loss coefficient U_{L} depends strongly on the time of the day (Fig. 1b and d). It is larger near the noon, when the plate temperature is usually larger. The coefficient U_{L} decreases by decreasing the inlet fluid temperature $T_{\text{f,i}}$ but this is not very obvious. The heat transfer coefficient h_{f} has an important time variation (Fig. 1a and c). Its hourly dependence is a function of the inlet fluid temperature $T_{\text{f,i}}$. When $T_{\text{f,i}}$ is high, the mass-flow rate is high near sunrise and sunset (when the inlet fluid temperature exceeds the ambient temperature). In this situation h_{f} is high in the beginning and end of the day (Fig. 1a). When lower values of $T_{\text{f,i}}$ are considered, the mass-flow rate is usually higher in the middle of the day, when the available amount of solar energy is also higher. In this case h_{f} has a maximum around the noon (Fig. 1c).

South oriented collectors are considered in this study. The (near) optimum tilt angle depends on the period of operation as follows. For warm season operation the collectors are tilted 20° while for cold season operation the collectors are tilted 55°.

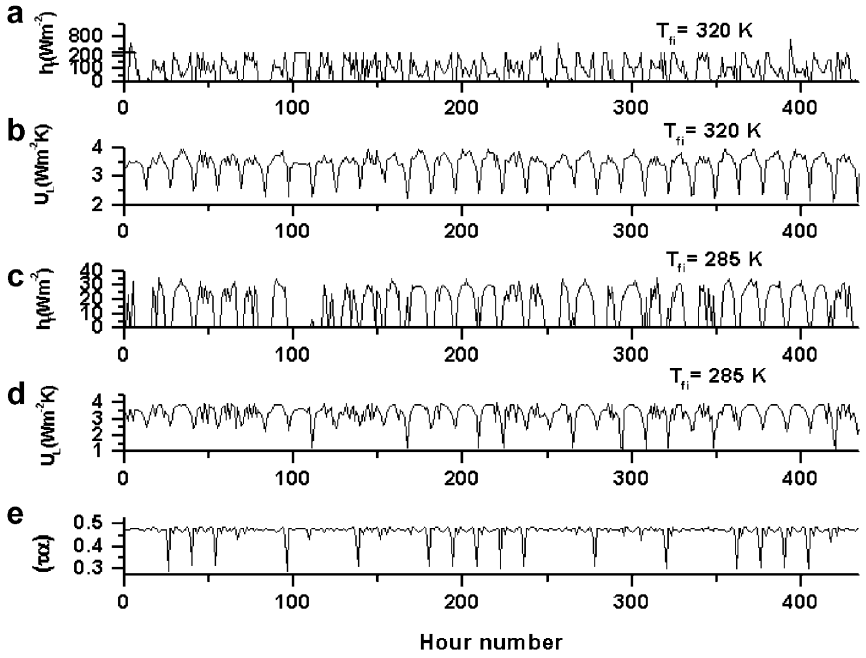

Fig. 1. Dependence of the heat transfer coefficient h_f ((a) and (c)) and overall heat loss coefficient U_L ((b) and (d)) on hour number in July, for two values of the inlet fluid temperature (i.e. $T_{f,i} = 285$ K and 320 K). The effective transmittance–absorptance product ($\tau\alpha$) is also shown in (e). Only hours during the daylight time are represented. This figure is associated to Fig. 5.

4. Optimum operation

The mechanical energy necessary to move the fluid is not considered here. Therefore, the exergy fluxes entering and leaving the collection area with the working fluid, $\dot{E}_{x,i}$ and $\dot{E}_{x,out}$, respectively, are given by

$$\dot{E}_{x,i(out)} = \dot{m}c_p T_{amb}\left(\frac{T_{f,i(out)} - T_{amb}}{T_{amb}} - \ln\frac{T_{f,i(out)}}{T_{amb}}\right) \tag{4}$$

The gained exergy flux $\dot{E}_x \equiv \dot{E}_{x,out} - \dot{E}_{x,i}$ may be evaluated by using Eq. (4). It is

$$\dot{E}_x = \dot{m}c_p T_{amb}\left(\frac{T_{f,out} - T_{f,i}}{T_{amb}} - \ln\frac{T_{f,out}}{T_{f,i}}\right) \tag{5}$$

The exergy E_x collected during the time period $t_1 - t_2$ is obtained by integration of Eq. (5):

$$E_x = A_c\int_{t_1}^{t_2}\left[\dot{m}'c_p T_{amb}\left(\frac{T_{f,out} - T_{f,i}}{T_{amb}} - \ln\frac{T_{f,out}}{T_{f,i}}\right)\right]dt \tag{6}$$

Here the definition of $\dot{m}'$ was also used.

The optimization problem consists of finding the optimum function $\dot{m}'_{opt}(t)$ that makes E_x given by Eq. (6) a maximum, taking account of the constraint equation (1). The time period $t_1 - t_2$ entering Eq. (6) normally refers to the interval between sunrise (t_1) and sunset (t_2). The usual assumption is that collector plate temperature at time t_1 equals the ambient temperature:

$$T(t = t_1) = T_{amb}(t = t_1) \tag{7}$$

Eq. (7) may be used as a boundary value when solving the ordinary differential equation (1). The following dimensionless quantities are defined:

$$\tau \equiv \frac{t}{t_{ref}}, \quad g \equiv \frac{G}{G_{ref}}, \quad \theta \equiv \frac{T}{T_{ref}}, \quad \theta_i \equiv \frac{T_{f,in}}{T_{ref}}, \quad \theta_{amb} \equiv \frac{T_{amb}}{T_{ref}} \tag{8a–e}$$

The subscript "ref" in Eqs. (8a–e) defines a constant quantity. Also, the following dimensionless quantities related to solar collector operation are defined:

$$(\widetilde{\tau\alpha}) \equiv \frac{(\tau\alpha)}{M'c_m}\frac{G_{ref}t_{ref}}{T_{ref}}, \quad \widetilde{U} \equiv \frac{U_L t_{ref}}{M'c_m}, \quad \tilde{h} \equiv \frac{h_f t_{ref}}{M'c_m},$$
$$\mu \equiv \left(\frac{1}{2} + \frac{\dot{m}c_p}{h_f A'_t}\right)^{-1} \tag{9a–d}$$

The quantity μ in Eq. (9d) is the dimensionless mass-flow rate factor, which is our new control function. Note that $(\widetilde{\tau\alpha})$, $\widetilde{U}$ and $\tilde{h}$ are time-dependent quantities. With notation equation (8), the objective function equation (6) becomes

$$\widetilde{E}_x \equiv \frac{E_x}{M'A_c c_m T_{ref}} = \int_{\tau_1}^{\tau_2}\theta_{amb}\tilde{h}\left(\frac{1}{\mu} - \frac{1}{2}\right)\left\{\mu\left(\frac{\theta - \theta_i}{\theta_{amb}}\right) - \ln\left[1 + \mu\left(\frac{\theta}{\theta_i} - 1\right)\right]\right\}d\tau \tag{10}$$

while the constraint equation (1) (sometimes referred to as the state equation) becomes

$$\frac{d\theta}{d\tau} = (\widetilde{\tau\alpha})g - \widetilde{U}(\theta - \theta_{amb}) - \tilde{h}\left(1 - \frac{\mu}{2}\right)(\theta - \theta_i) \tag{11}$$

Generally, the objective function $\widetilde{E}_x$ given by Eq. (10) may be seen as a function of θ, $d\theta/d\tau$ and μ and procedures of variational calculus may be used to find the optimum function $\mu_{opt}(\tau)$. Bejan [14] used such techniques to find the optimum mass-flow rate in a very specific case with additional simplifying assumptions. This case is shown for convenience in Section 4.1. However, the variational approach has no solution in the general case under similar simplifying assumptions (see Section 4.2). Thus, a direct optimal control technique is used to solve the problem in Section 4.3.

4.1. Variational approach for a simple case

The case studied in [14] is a particular case of our more general approach. The following simplifying assumptions are adopted: (i) $T_{f,out} = T$, (ii) $T_{f,i} = T_{amb}$, (iii) the characteristics of the solar collector do not depend on T and μ and (iv) the ambient temperature T_{amb} is constant in time and equals the reference temperature T_{ref} in Eqs. (8c–e).

Use of hypothesis (i) means $\mu = 1$. However, this simplification will be used only in the parentheses of Eq. (10), which becomes

$$\widetilde{E}_x = \int_{\tau_1}^{\tau_2} \theta_{amb} \tilde{h}\left(1-\frac{\mu}{2}\right)\left[\left(\frac{\theta-\theta_i}{\theta_{amb}}\right) - \ln\left(\frac{\theta}{\theta_i}\right)\right] d\tau \tag{12}$$

Now, $\tilde{h}(1-\mu/2)$ is extracted from Eq. (11)

$$\tilde{h}\left(1-\frac{\mu}{2}\right) = \frac{(\widetilde{\tau\alpha})g - \widetilde{U}(\theta-\theta_{amb}) - \frac{d\theta}{d\tau}}{\theta-\theta_{amb}} \tag{13}$$

and is replaced in Eq. (12), leading to

$$\widetilde{E}_x = \int_{\tau_1}^{\tau_2} F\left(\theta, \frac{d\theta}{d\tau}\right) \equiv \int_{\tau_1}^{\tau_2} \theta_{amb}\left\{\frac{(\widetilde{\tau\alpha})g - \widetilde{U}(\theta-\theta_{amb}) - \frac{d\theta}{d\tau}}{\theta-\theta_{amb}}\right\} \times \left[\left(\frac{\theta-\theta_i}{\theta_{amb}}\right) - \ln\left(\frac{\theta}{\theta_i}\right)\right] d\tau \tag{14}$$

The objective function given by Eq. (14) may be maximized by using the variational approach. A solution is found by solving the Euler–Lagrange equation:

$$\frac{\partial F}{\partial \theta} - \frac{d}{d\tau}\left[\frac{\partial F}{\partial(d\theta/d\tau)}\right] = 0 \tag{15}$$

Use of Eqs. (14) and (15) as well as the hypotheses (ii)–(iv) yield the following equation whose solution is the optimum dimensionless temperature θ_{opt}:

$$\frac{(\widetilde{\tau\alpha})g}{\widetilde{U}\theta_{amb}} = \frac{(\theta_{opt}-1)^3}{\theta_{opt}\ln\theta_{opt} - \theta_{opt} + 1} \tag{16}$$

This equation was first derived in [14]. Note that in Eq. (16) the parameter g (i.e. the solar global irradiance G) is allowed to vary. The previous relationships may be used in principle to build a flow rate "instantaneous" controller. Indeed, measuring the solar global irradiance G (or, in other words, knowing the function $g(\tau)$) allows to find $\theta_{opt}(\tau)$ from Eq. (16) and, finally, the optimum mass-flow rate parameter $\mu_{opt}(\tau)$ from Eq. (13). However, the four simplifying assumptions make this result of rather limited practical interest.

4.2. Variational approaches for the general case

From Eq. (11) one extracts $\tilde{h}(1-\mu/2)$ and replaces it in the dimensionless objective function equation (10), which becomes

$$\widetilde{E}_x = \int_{\tau_1}^{\tau_2} F'\left(\theta, \frac{d\theta}{d\tau}, \mu\right) d\tau \equiv \int_{\tau_1}^{\tau_2} \theta_{amb}\left\{\frac{(\widetilde{\tau\alpha})g - \widetilde{U}(\theta-\theta_{amb}) - \frac{d\theta}{d\tau}}{\theta-\theta_i}\right\} \times \left\{\left(\frac{\theta-\theta_i}{\theta_{amb}}\right) - \frac{1}{\mu}\ln\left[1+\mu\left(\frac{\theta}{\theta_i}-1\right)\right]\right\} d\tau \tag{17}$$

One sees that in the general case the objective function depends on both $\theta(\tau)$ and $\mu(\tau)$, as well as on $d\theta/d\tau$. The maximum of $\widetilde{E}_x$ is given by a specific functions $\theta_{opt}(\tau)$ and $\mu(\tau)$ which obey the Euler–Lagrange equations:

$$\frac{dF'}{d\theta} - \frac{d}{d\tau}\left[\frac{\partial F'}{\partial(d\theta/d\tau)}\right] = 0 \tag{18}$$

$$\frac{dF'}{d\mu} = 0 \tag{19}$$

The solar collector characteristic $\widetilde{U}$ depends in a very complicated manner on the parameters θ and μ. A way of making the problem tractable is to use the method of "frozen" parameters, which assumes the collectors parameters, as well as the dimensionless ambient temperature θ_{amb}, have a weaker time dependence than the variables θ and μ. Therefore, all these parameters are assumed to be constant in time. Then, the derivatives in Eqs. (18) and (19) may be easily performed by using Eq. (17) and the results are, respectively:

$$\frac{(\widetilde{\tau\alpha})g - \widetilde{U}(\theta-\theta_{amb})}{(\widetilde{\tau\alpha})g - \widetilde{U}(\theta_i-\theta_{amb})}\,\frac{\theta_i-\theta_{amb}+\mu(\theta-\theta_i)}{\theta_i+\mu(\theta-\theta_i)}\,\frac{\mu}{\theta_{amb}} = \frac{\mu\left(\frac{\theta-\theta_i}{\theta_{amb}}\right) - \ln\left[1+\mu\left(\frac{\theta}{\theta_i}-1\right)\right]}{\theta-\theta_i} \tag{20}$$

$$\left[1+\mu\left(\frac{\theta}{\theta_i}-1\right)\right]\ln\left[1+\mu\left(\frac{\theta}{\theta_i}-1\right)\right] - \mu\left(\frac{\theta}{\theta_i}-1\right) = 0 \tag{21}$$

Solving Eqs. (20) and (21) for the unknown function μ and θ would give the solution. Eq. (21) has the solution $\mu(\theta/\theta_i - 1) = 0$, which corresponds to $\mu_{opt} = 0$ or $\theta_{opt} = \theta_i$. In fact, the strategy $\mu_{opt} = 0$ (i.e. an infinitely large mass-flow rate) covers the case $\theta_{opt} = \theta_i$, too. But this strategy yields $\widetilde{E}_x = 0$ for the extreme of the objective function, which is useless from the point of view of practical applications.

Another approach is to try to eliminate μ from the parentheses in the integral of the r.h.s. member of Eq. (17). Fig. 2 (which refers to optimum operation during the warm season and $T_{f,i} = 285$ K) shows that $x \equiv \mu(\theta/\theta_i - 1)$ is generally smaller than 0.35. The x values are even smaller in case of higher inlet fluid temperature

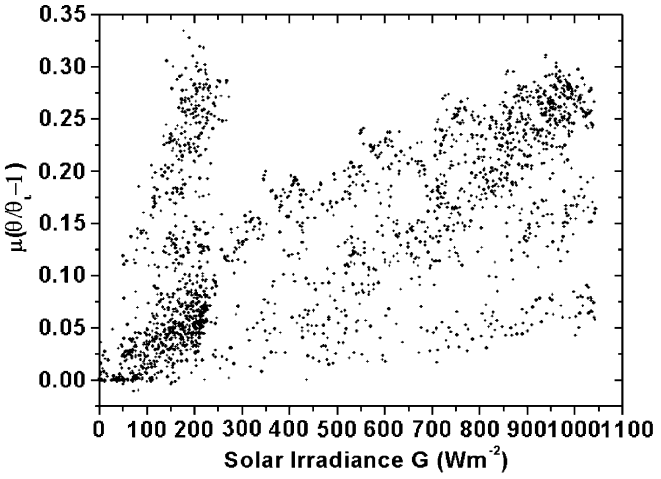

Fig. 2. Values of $\mu(\theta/\theta_i) - 1$ as function of solar global irradiance G. Hourly values for optimum operation during the warm season were considered. Inlet fluid temperature $T_{f,i} = 285$ K.

$T_{f,i}$ and/or optimum operation during the cold season. Therefore, x may be assumed in first approximation as a small parameter. Consequently, $\ln(1+x) \cong x$. This linearization procedure introduces relative errors smaller than 0.5%, 2.5%, 5%, 10%, 15% and 19% for x equals to 0.001, 0.005, 0.1, 0.2, 0.3 and 0.4, respectively. The linearization yields the following objective function:

$$\widetilde{E}_x = \int_{\tau_1}^{\tau_2} \left(1 - \frac{\theta_{amb}}{\theta_i}\right) \tilde{h} \left(1 - \frac{\mu}{2}\right) (\theta - \theta_i) d\tau \tag{22}$$

Use of Eqs. (13) and (22) finally yields

$$\widetilde{E}_x = \int_{\tau_1}^{\tau_2} F'' \left(\theta, \frac{d\theta}{d\tau}\right) d\tau \equiv \int_{\tau_1}^{\tau_2} \left(1 - \frac{\theta_{amb}}{\theta_i}\right) \left[(\widetilde{\tau\alpha}) g - \widetilde{U}(\theta - \theta_{amb}) - \frac{d\theta}{d\tau}\right] d\tau \tag{23}$$

The Euler–Lagrange equation associated to Eq. (23) is similar to Eq. (15). To make it tractable the method of the "frozen" parameters should be adopted. In this case, however, one can easily see that the Euler–Lagrange equation has no solution. One concludes that the variational approach yields no useful result in the general case, at least when the method of frozen parameters is adopted.

4.3. Direct optimal control approach

The optimization problem may be solved by using optimal control techniques. One may choose between indirect methods (such as those based on Pontryaghin principle) and direct methods. Indirect methods were already used in treating various heating and cooling processes (see e.g. [23–25]). They need preparing an adjoined (or co-state) differential equation to the state equation. This task is difficult to implement in the present case, mainly because of the implicit dependence of the Hamiltonian on the state variable θ. Indeed, the overall heat loss coefficient depends on the plate temperature. Accurate modeling should take account of this dependence (see e.g. [26]) which creates difficulties in computing the derivatives of the Hamiltonian over θ.

Here we used a direct shooting approach, i.e. trajectory optimization by mathematical programming (TOMP) [27]. This avoids the need for the co-state equation by transforming the original optimal control problem into a nonlinear programming problem (NPP). The basic ideas of the numerical TOMP algorithm are presented next. The state equation (11) and the relation (7) represent an initial value problem (IVP) as a sub-problem. The integration time interval in Eq. (10) is divided into-sub-intervals separated by nodes. The values of the control parameter (i.e. μ) in these nodes constitute the so called parameter vector. Initially, this parameter vector is unknown and a guess is necessary. The IVP is solved on the above integration interval by using common Runge–Kutta techniques. The resulted values of the state variable in the nodes of the integration interval depend of course on the parameter vector. Consequently, the objective function equation (10) is dependent on this parameter vector. The NPP consists in maximizing the objective function in terms of the parameter vector. The resulted optimized parameter vector is returned as an entry to the IVP and a new set of values of the state variables in the nodes of the integration interval is obtained. Then, the objective function is maximized again and a new optimized parameter vector is obtained. This process continues until a given convergence condition for the parameter vector is satisfied. The software package TOMP is split into two modules, the simulator d_TOMP and the optimizer SLSQP which exchange their information by reverse communication. In d_TOMP the IVP is integrated. In SLSQP the NPP is solved by sequential linear least squares. More details may be found in [27].

All optimal control calculations reported next are done on a day by day basis, between sunrise and sunset. During the night the temperature of the flat-plate collector decreases towards the ambient temperature. Therefore, each day the plate temperature at sunrise equals the ambient temperature (see Eq. (7)). To increase the integration accuracy, the daylight interval was divided into a number of hourly sub-intervals. Integration was effectively performed on these hourly intervals. The following values were used in Eqs. (8): $t_{ref} = 3600$ s, $T_{ref} = 300$ K and $G_{ref} = 1000$ W m^{-2}.

5. Optimum operation

Several indicators of performance may be defined for the solar energy collection system as follows. The instantaneous and averaged energetic efficiency, η_{en} and $\bar{\eta}_{en}$, respectively, is given by

$$\eta_{en} \equiv \frac{\dot{m}' c_p (T_{f,out} - T_{f,i})}{G} \tag{24}$$

$$\bar{\eta}_{en} \equiv \frac{\int_{t_1}^{t_2} \dot{m}' c_p (T_{f,out} - T_{f,i})\, dt}{G(t_2 - t_1)} \tag{25}$$

Also, the instantaneous and averaged exergetic efficiency, η_{ex} and $\bar{\eta}_{ex}$, respectively, is given by

$$\eta_{ex} \equiv \frac{\dot{E}_x}{A_c G} \tag{26}$$

$$\bar{\eta}_{ex} \equiv \frac{E_x}{A_c G(t_2 - t_1)} \tag{27}$$

A brief presentation of some experimental results reported in literature may give perspective for our findings. The upper limit of unconcentrated solar radiation energy conversion into work on Earth surface is about 5.3% (for an ambient temperature of 300 K) [3]. Experimentally derived values may be found from two studies of combined systems consisting in heat pumps and flat-plate solar collectors [28,29]. The results in [28] were obtained in Trabzon, Turkey (41° N latitude). The 18 solar collectors are oriented south and tilted 40°. Each collector has 1.66 m^2 surface area and eight 1.25 cm outside diameter copper tubes spaced 10 cm apart. The aluminum flat-plate sheet is 0.55 mm thick and its absorptance is 0.8. The single glazing is 3.5 mm thick glass with 0.85 transmittance. The mass-flow rate through the collectors is 1300 kg h^{-1} ($\dot{m}' = 0.012$ kg m^{-2} s^{-1}). The exergetic efficiency of solar collectors is defined in [28] as the ratio between the exergy gain and the maximum theoretically possible exergy gain. Figs. 5–7 in [28] show this exergetic efficiency ranges between 25% and 50%. To convert these values into exergetic efficiency values defined by Eqs. (26) and (27) they should be multiplied by 5.3%. The resulting values range between 1.32% and 2.65%. An uncovered solar collector with 4.5 m^2 surface area was studied in [29]. No details about the mass-flow rate are given. The authors defined the exergetic efficiency of the whole combination solar collectors–heat pump. The experimental results are shown in their Fig. 2. The exergetic efficiency ranges between 1% and 4%. Another experimental study refers to a solar power plant based on low-temperature technology [26]. This plant is located in Borj Cedria, a small sea-side town 20 km south of Tunis. The unit has a 720 m^2 array of flat-plate collectors (of the water-heater type) linked to a 45 m^3 water storage tank. The stored thermal energy is transformed into electricity by using a 10-kW turbo-alternator station connected to the electrical grid. The efficiency of the plant is low. During the hot season, it is in the order of 2%. When the weather is bad, the plant does not operate. Two different periods were distinguished. The first extends from April to October, when the turbine is able to work 8 h per day. The second period characterizes the cold season, when the turbine can not operate more than 2 h a day.

Our results are reported now. They are obtained by using the direct optimal control technique described in Section 4.3. Fig. 3a shows that in January the exergetic efficiency η_{ex} is low (less than 3%), as expected. The time variation of η_{ex} is rather well correlated to the time variation of solar global irradiance G (Fig. 3c). This is in good concordance with early results by Bejan [14]. There is no obvious correlation between the time evolution of η_{ex} and ambient temperature T_{amb} (Fig. 3d). It is not easy to find by visual inspection a correlation between the time dependence of the optimum mass-flow rate $\dot{m}'$ (Fig. 3b) and G or T_{amb}. However, a closer inspection shows that the highest values of $\dot{m}'$ occur near sunrise and sunset. Note that high values of η_{ex} corresponds to low values of $\dot{m}'$ (compare Fig. 3a and b).

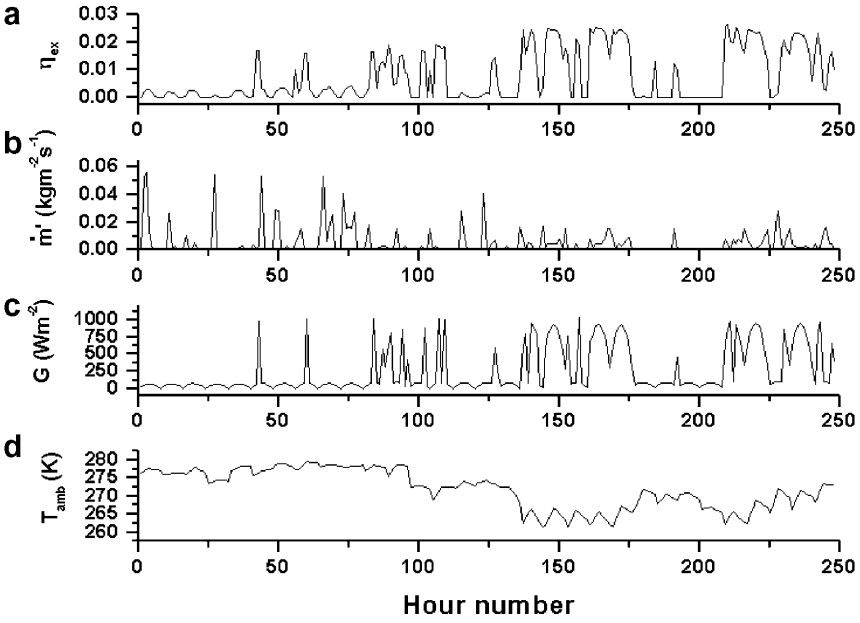

Fig. 3. Dependence of some meteorological and operational parameters on hour number in January: (a) the energetic efficiency η_{en}; (b) the optimum mass-flow rate $\dot{m}'$ per unit collector surface area; (c) the global solar irradiance G incident on the collector; (d) ambient temperature T_{amb}. Only hours during daylight time are represented. The inlet fluid temperature is $T_{f,i} = 285$ K.

In case the objective function is the collected solar energy, the early work [9] proved that the optimal operation strategy requires using the maximum possible mass-flow rate. This applies to open loop systems but only during those time periods when the collector provides a non-null flux of useful thermal energy. Additional constraints should be fulfilled in case of solar energy systems with stratified storage.

Fig. 4 shows that the optimum mass-flow rate $\dot{m}'$ increases significantly when increasing the fluid inlet temperature $T_{f,i}$. At high values of $T_{f,i}$ (Fig. 4a) the average of the cloud of $\dot{m}'$ data is about 0.01 kg m^{-2} s^{-1}, which is of the order of values used in practice today. For example, values between 0.0042 and 0.0236 kg m^{-2} s^{-1} were adopted in a study dealing with modeling variable mass-flow rate collectors [30].

The data cloud in Fig. 4a has a rather high dispersion. When lower values of $T_{f,i}$ are considered (Fig. 4b) the average mass-flow rate per unit surface area is about ten times lower than the values used in practice today. Both data clouds in Fig. 4 are vertically distributed and this means that $\dot{m}'$ is weakly correlated with ambient temperature, whatever the value of the inlet fluid temperature is.

Fig. 5 shows that in July the mass-flow rate per unit surface area $\dot{m}'$ is rather well correlated with global solar irradiance G, whatever the value of $T_{f,i}$ is. Increasing $T_{f,i}$ makes $\dot{m}'$ to increase. Generally, $\dot{m}'$ reaches its maximum near sunrise and sunset. This is more obvious in Fig. 5b and c, associated to higher values of $T_{f,i}$. In the middle of the day $\dot{m}'$ is rather constant. This is again more obvious in Fig. 5b and c.

6. Aspects of controller design

Controllers in solar energy collection systems are differentiated upon objective, complexity and way of operation.

In case of closed loop solar thermal systems the typical control system has one sensor mounted on the collector absorber plate near the fluid outlet and another mounted in the bottom of the storage tank. With no flow through the collector, the collector sensor essentially measures the mean plate temperature. With flow, the collector sensor measures the outlet fluid temperature. The optimal condition for the controller is simply to turn on the pumps when the value of the solar energy that is delivered to the load just exceeds the value of the energy needed to operate the pump [31].

In case of solar space heating applications the usual classification of controllers is as follows. Controllers of first kind (also called distribution controllers) allow optimal heat distribution in a building. This means that a certain objective function related to the thermal energy provided or living discomfort is minimized. Controllers of second kind (collection controllers) maximize the difference between the useful collected energy and the energy required to transport the working fluid. The controllers of third kind combine collection and distribution functions [32]. The second kind controllers are responsible for the optimum operation of the pumps. Two sorts of second kind controllers are often used in applications. One is the bang–bang controller (the mass-flow rate has two allowable values: maximum and zero). The other is the proportional controller (the mass-flow rate is a linear function of the difference

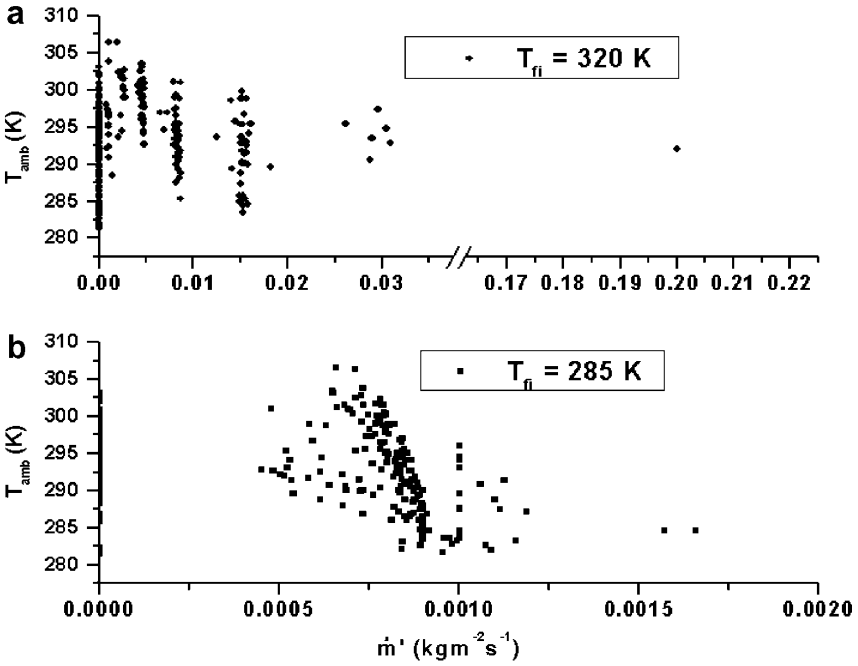

Fig. 4. Dependence of the optimum mass-flow rate $\dot{m}'$ per unit collector surface area on ambient temperature T_{amb} during the warm season for two values of the inlet fluid temperature: (a) $T_{f,i} = 320$ K; (b) $T_{f,i} = 285$ K.

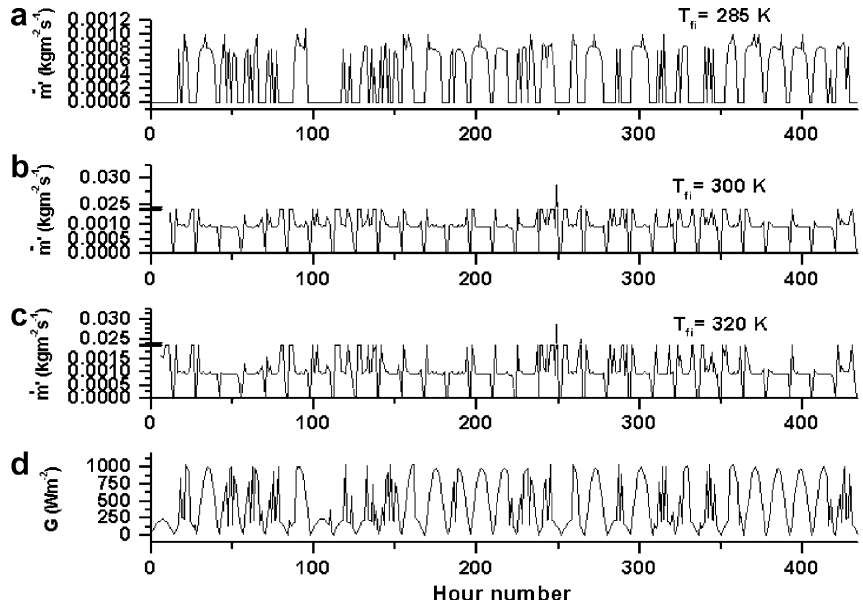

Fig. 5. Dependence of the optimum mass-flow rate $\dot{m}'$ per unit collector surface area on hour number in July for different values of the inlet fluid temperature: (a) $T_{f,i} = 285$ K; (b) $T_{f,i} = 300$ K; (c) $T_{f,i} = 320$ K. The dependence of the incident solar global irradiance on the hour number is also shown in (d). Only hours during the daylight time are represented.

between the outlet working fluid temperature and the temperature inside the storage tank). Variants of proportional controllers exist such as PID (proportional integral plus derivative mode) and PSD (proportional sum derivative) controllers [15].

In case of systems for work generation a different control strategy is usually adopted. Published studies concerning solar thermal power plant operation consider that the purpose of the control is to regulate the outlet temperature of the collector field by suitable adjusting the working fluid flow [33–36].

Designing a mass-flow rate controller based on optimal control theory encounters a major difficulty: one needs a priori knowledge of meteorological data time series. An

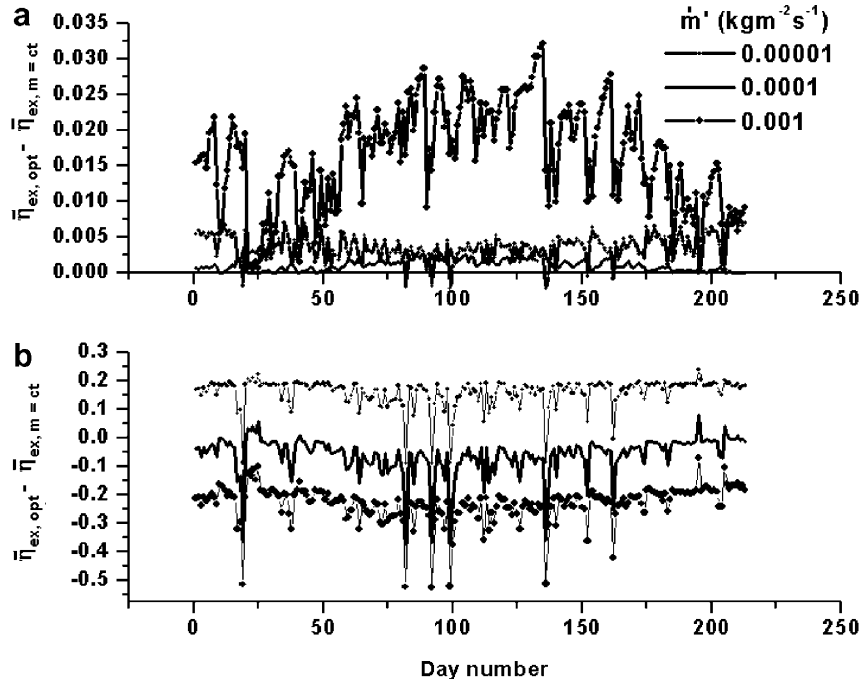

Fig. 6. Difference between values of daily average exergetic efficiency $\bar{\eta}_{ex}$ (a) and daily average energetic efficiency $\bar{\eta}_{en}$ (b) for four strategies of solar energy collection, i.e. optimum mass-flow rate (opt) and three different constant mass-flow rates ($m = ct$). All the days of the warm season were considered. The inlet fluid temperature is $T_{f,i} = 285$ K.

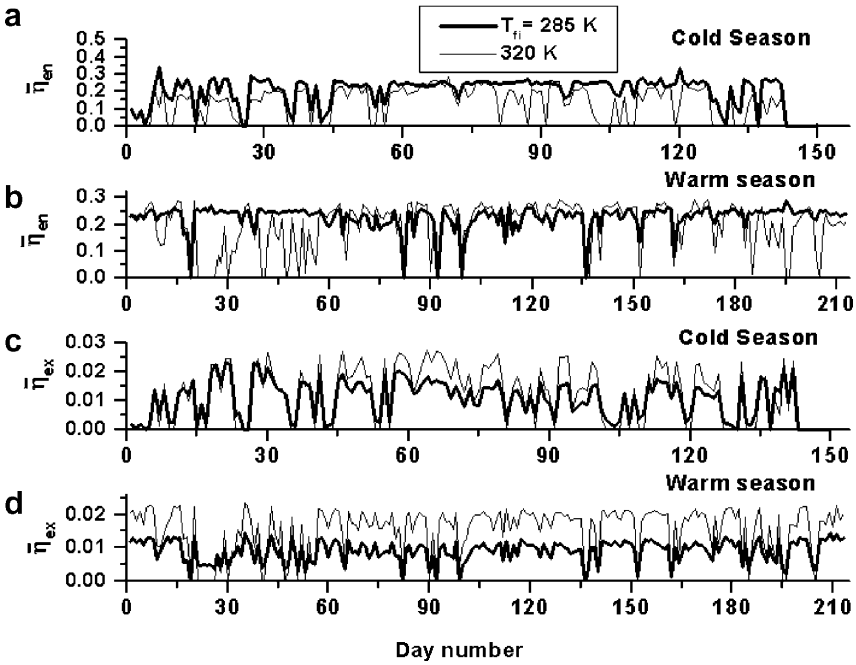

Fig. 7. Dependence of the daily average energetic efficiency $\bar{\eta}_{en}$ ((a) and (b)) and daily average exergetic efficiency $\bar{\eta}_{ex}$ ((c) and (d)) on day number during the cold and warm seasons. Two values of the inlet fluid temperature were considered, i.e. $T_{f,i} = 285$ K and 320 K, respectively.

"instantaneous" controller, able to optimally adjust the mass-flow rate by using as input just the last (in time) measured value of the meteorological parameters, would be highly desirable. This would avoid modeling the future history of irradiance and ambient temperature. In Section 4.1 we showed that Bejan [14] used variational methods and obtained a relationship that allows such an "instantaneous" controller to be build. However, the case studied in [14] is very simple and the additional simplifications make the results of little practical interest.

Results of Fig. 5 suggest that a constant mass-flow rate may be a good strategy during the warm season. Fig. 6a shows the difference between the values of the daily averaged exergetic efficiency $\bar{\eta}_{ex}$ obtained by using the optimal control strategy $\dot{m}'_{opt}$ and three strategies based on a constant mass-flow rate, respectively. The strategy using the constant value $\dot{m}' = 0.0001$ kg m^{-2} s^{-1} yields results very close to the optimum. The other two constant mass-flow rate strategies give worse results. One of them (i.e. $\dot{m}' = 0.001$ kg m^{-2} s^{-1}) is sometime associated to negative values of $\bar{\eta}_{ex}$. Fig. 6b shows results for the daily averaged energetic efficiency $\bar{\eta}_{en}$ associated to the four strategies of Fig. 6a. The energetic efficiency increases by increasing the mass-flow rate, as expected. Obviously, the strategy of maximum exergy collection is different from that of maximum energy collection.

Fig. 7 shows the daily averaged values of the energetic and exergetic efficiencies, $\bar{\eta}_{en}$ and $\bar{\eta}_{ex}$, respectively, during the cold and warm season, for two values of the inlet fluid temperature $T_{f,i}$. All these values are associated to the mass-flow rate $\dot{m}'_{opt}$ that maximizes exergy collection. The energetic efficiency $\bar{\eta}_{en}$ is generally smaller than 0.35 whatever the season is (Fig. 7a and b). Note that energetic efficiency values higher than 0.5 are usual for actual flat-plate collector technology. The lower performance reported here is a result of using a different objective function (i.e. exergy gain instead of energy gain). Generally, $\bar{\eta}_{en}$ decreases when $T_{f,i}$ increases, in agreement with current practice. The daily averaged exergetic efficiency $\bar{\eta}_{ex}$ is generally lower than 0.03 and obviously increases when $T_{f,i}$ increases (Fig. 7c and d). A more constant in time performance is observed during the warm season.

7. Conclusions

Solar collectors are now largely used in industry, civil engineering and other activities. The control of temperature and flow rates in solar thermal engineering is an important factor for performance increasing. Some authors stated that, in many instances, energy-based performance measures can be misleading, and that exergy-based performance measures provide a more realistic evaluation of thermodynamic systems [8]. Exergy analysis is, indeed, a useful mean for understanding how we use energy to perform a specific task. For instance, analysis of exergy flows in solar-driven systems can lead to identification of inefficient parts and optimum operating conditions.

This paper refers to optimal operation strategies for exergy gain maximization in open loop thermal solar energy collection systems. The water mass-flow rate in the collectors is the control parameter. The main contributions consist in improving the energy conversion model and the solar collector model. Also, an optimal control approach was adopted here instead of the variational

approach used in previous work. Indirect optimal control methods are rather difficult to implement because explicit adjoined equations cannot be easily built for the realistic flat-plate solar collector model adopted in the present work. A direct method (the TOMP algorithm) was used to find the optimal paths.

A large meteorological database was used in calculations. Optimum tilted south oriented collectors were considered. Simulations were performed for both warm and cold season operation. The maximum exergetic efficiency is low (usually less than 3%), in rather good concordance with experimental measurement reported in literature.

No obvious correlation was found during the cold season between the optimum mass-flow rate $\dot{m}'$ and the ambient temperature. The highest values of $\dot{m}'$ occur near sunrise and sunset. Also, the optimum mass-flow rate increases significantly when increasing the fluid inlet temperature. During the warm season the optimum mass-flow rate is well correlated with the global solar irradiance. Also, $\dot{m}'$ is rather constant in the middle of the day.

The controller purpose in present-day solar thermal power plants is to regulate the outlet temperature of the collector field by suitable adjusting the working fluid flow [36]. This may ensure a smooth operation but is not necessarily associated to maximum exergy extraction. The method proposed here allows finding the optimal paths but it has the obvious disadvantage that requires a priori knowledge of meteorological data time series.

An "instantaneous" controller, able to optimally adjust the mass-flow rate by using as inputs just the last (in time) measured values of the meteorological parameters is difficult to build. Instead, operation at constant mass-flow rate may be useful, at least during the warm season. The particular value of the mass-flow rate to be used may be found by comparing results obtained by using the optimal control theory and constant mass-flow rate operation, respectively, both of them using as input time series of measured meteorological data from previous years.

Acknowledgement

The author thanks the referee for useful remarks and suggestions.

References

[1] R. Petela, Exergy of undiluted thermal radiation, Solar Energy 74 (6) (2003) 469–488.
[2] V. Badescu, Letter to the editor, Solar Energy 76 (2004) 509–511.
[3] V. Badescu, Maximum conversion efficiency for the utilization of multiply scattered solar radiation, J. Phys. D: Appl. Phys. 24 (1991) 1882–1885.
[4] M. Izquierdo, M. De Vega, A. Lecuona, P. Rodriguez, Compressors driven by thermal solar energy: entropy generated, exergy destroyed and exergetic efficiency, Solar Energy 72 (4) (2002) 363–375.
[5] A. Bejan, Entropy Generation Through Heat and Fluid Flow, Wiley, New York, 1982.
[6] V. Badescu, First and second law analysis of a solar assisted heat pump based heating system, Energy Convers. Manage. 43 (2002) 2539–2552.
[7] V. Badescu, Model of a solar-assisted heat-pump system for space heating integrating a thermal energy storage unit, Energy Build. 34 (2002) 715–726.
[8] L.H. Gunnewiek, S. Nguyen, M.A. Rosen, Evaluation of the optimum discharge period for closed thermal energy storages using energy and exergy analyses, Solar Energy 51 (1) (1993) 39–43.
[9] M. Kovarik, P.F. Lesse, Optimal control of flow in low temperature solar heat collectors, Solar Energy 18 (5) (1976) 431–435.
[10] J.D. Horel, F. De Winter, Investigations of methods to transfer heat from solar liquid-heating collectors to heat storage tanks. Final report on US Department of Energy Contract E(04)1238, Altas Corporation, Santa Cruz CA, April 1978.
[11] A. Bejan, W. Schultz, Optimum flow-rate history for cooldown and energy storage processes, Int. J. Heat Mass Transfer 25 (8) (1982) 1087–1092.
[12] K.G.T. Hollands, A.P. Brunger, Optimum flow rates in solar water heating systems with a counterflow exchanger, Solar Energy 48 (1) (1992) 15.
[13] F. De Winter, Comments on optimum flow rates in solar water heating systems with a counterflow exchanger, Solar Energy 49 (6) (1992) 557–558.
[14] A. Bejan, Extraction of exergy from solar collectors under time-varying conditions, Int. J. Heat Fluid Flow 3 (2) (1982) 67–72.
[15] A. Morteza, M. Ardehali, K.H. Yae, T.F. Smith, Development of proportional-sum-derivative control methodology, Solar Energy 57 (4) (1996) 251–260.
[16] Anuarul meteorologic, Institutul de Meteorologie si Hidrologie, Bucuresti, 1961 (in Romanian).
[17] V. Badescu, A new kind of cloudy sky model to compute instantaneous values of diffuse and global solar irradiance, Theor. Appl. Climatol. 72 (2002) 127–135.
[18] C. Oancea, E. Zamfir, C. Gheorghita, Studiul aportului de energie solara pe suprafete plane de captare cu orientari si unghiuri de inclinare diferite, Energetica 29 (1981) 451–456 (in Romanian).
[19] V. Badescu, Can the BCLS model be used to compute the global solar radiation on the Romanian territory? Solar Energy 38 (1987) 247–254.
[20] M. Gazela, E. Mathioulakis, A new method for typical weather data selection to evaluate long-term performance of solar energy systems, Solar Energy 70 (2001) 339–348.
[21] J.A. Duffie, W.A. Beckman, Solar Energy Thermal Processes, Wiley, New York, 1974.
[22] V. Badescu, Optimum fin geometry in flat plate solar collector systems, Energy Convers. Manage. 47 (2006) 2397–2413.
[23] V. Badescu, Optimal control of forced cool-down processes, Int. J. Heat Mass Transfer 48 (2005) 741–748.
[24] V. Badescu, Optimal strategies for steady state heat exchanger operation, J. Phys. D: Appl. Phys. 37 (2004) 2298–2304.
[25] V. Badescu, Optimal paths for minimizing lost available work during usual heat transfer processes, J. Non-Equil. Thermodyn. 29 (2004) 53–73.
[26] M. Chaabene, M. Annabi, A dynamic model for predicting solar plant performance and optimum control, Energy 22 (6) (1997) 567–578.
[27] D. Kraft, Algorithm 733: TOMP – Fortran modules for optimal control calculations, ACM Trans. Math. Software 20 (3) (1994) 262–281.
[28] K. Kaygusuz, T. Ayhan, Exergy analysis of solar-assisted heat-pump systems for domestic heating, Energy 18 (10) (1993) 1077–1085.
[29] E. Torres Reyes, M. Picon Nunez, J. Cervantes de Gortari, Exergy analysis and optimization of a solar assisted heat pump, Energy 23 (4) (1998) 337–344.
[30] F. Hilmer, K. Vajen, A. Ratka, H. Ackermann, W. Fuhs, O. Melsheimer, Numerical solution and validation of a dynamic model of solar collectors working with varying fluid flow, Solar Energy 65 (5) (1999) 305–321.

[31] W.A. Beckman, J. Thornton, S. Long, B.D. Wood, Control problems in solar domestic hot water systems, Solar Energy 53 (3) (1994) 233–236.
[32] C. Byron Winn, D. Ellsworth Hull III, Optimal controllers of the second kind, Solar Energy 23 (1979) 529–534.
[33] A. Meaburn, F.M. Hughes, Prescheduled adaptive control scheme for resonance cancellation of a distributed solar collector field, Solar Energy 52 (2) (1994) 155–166.
[34] S. Zunft, Temperature control of a distributed collector field, Solar Energy 55 (4) (1995) 321–325.
[35] R. Kohne, K. Oertel, S. Zunft, Investigation of control and simulation of solar process heat plants using a flexible test facility, Solar Energy 56 (2) (1996) 169–182.
[36] A. Meaburn, F.M. Hughes, A simple predictive controller for use on large scale arrays of parabolic trough collectors, Solar Energy 56 (6) (1996) 583–595.